

AOTF-based system for image cytometry

Bartek Rajwa^a, Wamiq Ahmed^a, Murugesan Venkatapathi^a, Gerald Gregori^a, Feng Jin^b, Jolanta Soos^b, Sudhir Trivedi^b, and J. Paul Robinson^{a*}

^aPurdue University Cytometry Laboratories, 201 S. University Street, West Lafayette, IN 47907

^bBrimrose Corporation of America, 19 Loveton Circle, Baltimore, MD 21152

ABSTRACT

This paper describes a simple, inexpensive multispectral imaging system for image cytometry applications. The system is based on an acousto-optical tunable filter (AOTF), a monochrome CCD camera, and a research-grade fluorescence microscope. The selected TeO₂ AOTF has a 10x10 mm² entrance aperture and operates within the spectral range of 447–750 nm. The bandpass of the filter varies between 1.4 nm at 450 nm and 5.1 nm at 690 nm. The control software works within the environment of a popular image-acquisition and -processing package Image Pro-Plus, making this system easy to integrate with many existing fluorescence microscopes and cameras. Since image-cytometry applications do not require very high spatial resolution, AOTF-based systems may become an interesting alternative to more complex and expensive LCTF or pushbroom methods.

Keywords: multispectral imaging, cytometry, AOTF

1. INTRODUCTION

The current surge of interest in multispectral flow cytometry has brought about a number of interesting designs ranging from systems based on linear CCD elements¹ to cytometers utilizing multianode PMTs^{2,3}. Verification of multispectral flow-cytometry results by independent microscopy-based systems is required both for development of these next generation technologies, and for routine use in future. Currently available multispectral imaging systems are usually complex and/or very expensive, and there are only a few successful implementations. The four main technologies used for biological multispectral imaging are Lyot filter-based liquid-crystal tunable filters (LCTF)^{4,6}, Fourier-transformed interferometry (FTI), pushbroom imagers (2-dimensional imaging spectrometers)^{7,8}, and whiskbroom (raster-scanning) multispectral devices – usually part of confocal instruments⁹. Although these technologies have been successfully integrated with commercially available instruments (Nuance from CRI, PARISS imaging spectrometer from Lightform, Meta detector from Zeiss, etc), several important limitations are apparent, such as limited spectral range and spectral resolution (PMT-based solution from Zeiss), low transmittance/sensitivity (LCTF), low throughput (pushbroom methods), and last but not least, high cost (all these instruments). The main reason for the high cost and complexity of these instruments is the fact that they offer very high spatial resolution and custom-built acquisition software. In this paper we report the use of an acousto-optical tunable filter integrated with a popular image-acquisition/processing package. This provides an inexpensive alternative for fast, mid-resolution, multispectral data collection. Since image cytometry applications do not require very high spatial resolution, an inexpensive low-aperture AOTF integrated with a monochrome CCD and a research-grade microscope may be the ideal solution. Our system differs from other instruments in two main aspects: the use of an off-the-shelf, inexpensive tunable filter, and the extendable control and analysis software working in the environment of a popular acquisition package. The whole system can be mounted on any fluorescence microscope and can be controlled by a laptop computer equipped with USB or serial port.

2. OPERATION OF AOTF FILTERS

Operation of the AOTF relies on the interaction of light and acoustic waves as both travel inside a birefringent crystal¹⁰. The density of the atoms making up the crystal is modulated by the acoustic or pressure wave. This results in modulation of the refractive index, which is directly affected by the structure of the atoms. Therefore, a volume grating is formed and moves with the speed of sound inside the crystal. Thus, certain wavelengths of light are diffracted to one or more orders. This phenomenon has been recognized for a very long time. In 1921 Brillouin predicted that a liquid traversed by ultrasonic compression waves would give rise, when irradiated with light, to diffraction. The first

* jpr@flowcyt.cyto.purdue.edu; phone: (765) 494 0757; fax: (765) 494 0517

observations of the AO phenomenon were reported in the 1930's by the Americans Debye and Sears, and independently by French scientists, Lucas and Biquard. The construction of the first collinear AOTF by Harris and Wallace was reported in 1969¹¹. An AOTF working in so-called non-collinear configuration, where the acoustic and optical waves propagate at quite different angles through the crystal, was reported in 1975 by Chang¹².

The most common choice of material for the AOTF is TeO₂, which is very efficient with a relatively large acousto-optic figure of merit and is transparent up to 5.5 μm. The first paratellurite AOTF was built by Yano and Watanabe in 1976¹³. TeO₂-based AOTFs are usually designed in a non-collinear configuration. When the zero-order beam is used as output, the AOTF functions as a notch filter; if the ±1-order beam is used, the AOTF functions as a bandpass filter. Figure 1 is a schematic representation of a non-collinear TeO₂ AOTF.

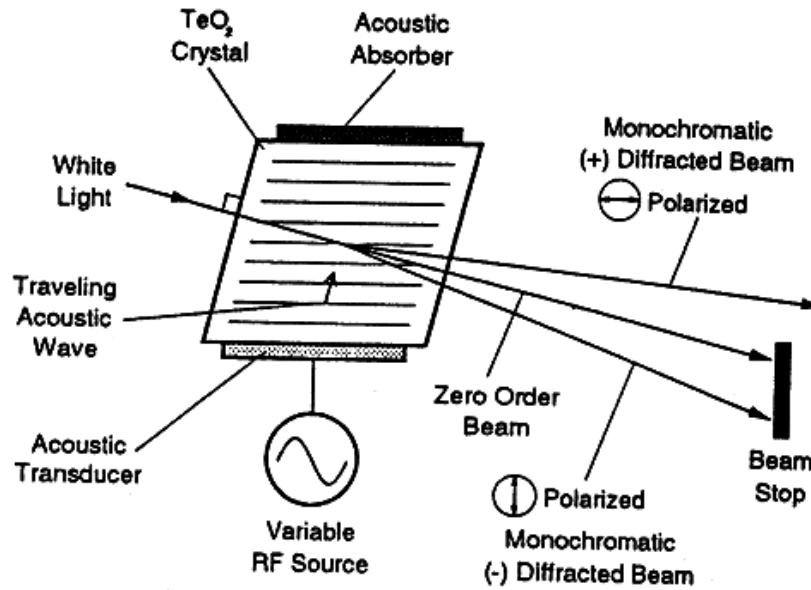


Figure 1 Schematic representation of a non-collinear paratellurite AOTF.

Several parameters are usually used to describe the characteristics of an AOTF – center wavelength λ_0 , line shape function, peak transmission T_0 , and spectral resolution $\Delta\lambda$.

The tuning relation between the center optical wavelength λ_0 of the optical passband and the frequency of the acoustic wave f_a is given by

$$\lambda_0 = \frac{V_a \Delta n}{f_a} \sqrt{\sin^4 \theta_i + \sin^2 2\theta_i} \quad (1)$$

where V_a is the speed of the acoustic wave traveling in the crystal, $\Delta n = n_e - n_o$ is the optical birefringence (n_e and n_o are the refractive indices between the extraordinary and ordinary lights, respectively), and θ_i is defined as the angle between the optical axis and the incident light.

The normalized line shape function of the passband is given by

$$T = \sin^2 \left(\frac{\Delta k L}{2\pi} \right) / \left(\frac{\Delta k L}{2\pi} \right)^2 \quad (2)$$

where T is the transmission normalized to peak transmission T_0 (described below), Δk is the wave number difference between the current wavelength and the center wavelength λ_0 , and L is the interaction length.

The peak transmission T_0 is given by the ratio of diffracted light to that of incident light, whose value is calculated as

$$T_0 = \sin^2 \left(\frac{\pi^2 M_2}{2\lambda_0^2} P_d L^2 \right)^{1/2} \quad (3)$$

P_d is the acoustic power density, given by

$$P_d = \frac{P}{H \times L} \quad (4)$$

where P is the acoustic power, H and L are the width and length, respectively, and M_2 is the acousto-optic figure of merit, expressed as

$$M_2 = \frac{n^6}{\rho V_a^3} p^2 \quad (5)$$

where n is the refractive index of the crystal, ρ is the density of the crystal, and p is the photoelastic constant.

The spectral resolution $\Delta\lambda$ of the tunable filter is given by

$$\Delta\lambda = \frac{1.8\pi\lambda_0^2}{bL\sin^2\theta_i} \quad (6)$$

where b is the dispersion constant given by

$$b = 2\pi(\Delta n - \lambda_0 \frac{\partial \Delta n}{\partial \lambda_0}) \approx 2\pi\Delta n \quad (7)$$

Many of the performance characteristics of an AOTF can be explained by the above equations. Equation (1) indicates that after the AOTF is designed and the incident angle θ_i is fixed, the center wavelength of the filter is controlled by the RF frequency applied to the transducer. This allows fast tuning, random access, and robustness. The line shape of the filter is the square of a sine function (equation 2) when the shape of the transducer is rectangular. It is possible to remove the side lobes of the line shape by using transducers of different shapes. The peak transmission T_0 can be optimized by selecting appropriate acoustic power and transducer length. The interaction length L plays a major role in determining the spectral resolution $\Delta\lambda$ of the AOTF. High resolution can be obtained by using a long crystal and transducer. Although the line shape of each AOTF is sine or triangular like, multiple filters can be combined together so that a single bandpass filter with a flat top is formed to minimize the distortion of spectral information.

3. AOTF-BASED IMAGING SYSTEM

3.1. AOTF, microscope, and camera

Paratellurite acousto-optical filters are well suited for microscopic imaging. The simple setup requires a collimated fluorescence signal to be directed through an AOTF tuned to the frequency corresponding to the wavelength of interest, and focused on a monochrome CCD chip. Multi- or hyperspectral spectral images can be obtained by collecting a series of monochrome images at different AOTF frequencies. Our AOTF-imaging system was based on a Brimrose TeO₂ tunable filter with a 10x10 mm² entrance aperture and a separation angle of ~7 degrees. The operating wavelength of the filter is 447–750 nm, the peak diffraction efficiency reaches ~70%. The bandpass of the filter depends on wavelength and increases as a function of λ^2 , varying between 1.4 nm at 450 nm and 5.1 nm at 690 nm. The tuning of the filter was controlled by frequencies between 90 and 185 MHz generated by the oscillator. The AOTF was mounted on a Nikon E-1000 motorized microscope, and monochrome images were collected using a QImaging Retiga 1300 camera (with Sony ICX085 chip). A PC computer running Media Cybernetics Image Pro-Plus 5.1 (IPP) software controlled the whole system, including the microscope, the camera, and the AOTF.

3.2. Control software

Our AOTF control software (IPP plug-in) operates within the environment of the IPP package. IPP plug-ins, extending the functionality of IPP, can be created with the IPP software development kit (SDK), which is distributed free by

Media Cybernetics. The SDK allows development of custom-built plug-in modules using many popular programming languages, including C++ and Visual Basic. Our acquisition and analysis module was built as such a plug-in; therefore it can utilize all the functionality of IPP, including its ability to control most motorized microscopes, stages and cameras. The current version of our software offers the following features:

1. Capability to automatically collect a number of monochrome images over a pre-defined spectral range
2. Previewing spectra from any pixel, and rectangular, oval, or irregular area of interests
3. Linear spectral un-mixing using previously collected spectra of single fluorochromes
4. Automated pixel classification upon their spectra using simple Euclidean distances or PCA analysis
5. Automated image shift correction. (A wavelength-dependent image shift occurs for AOTFs arising from spectral dispersion in the anisotropic crystal. However, the shift is reproducible and can be easily calculated.)

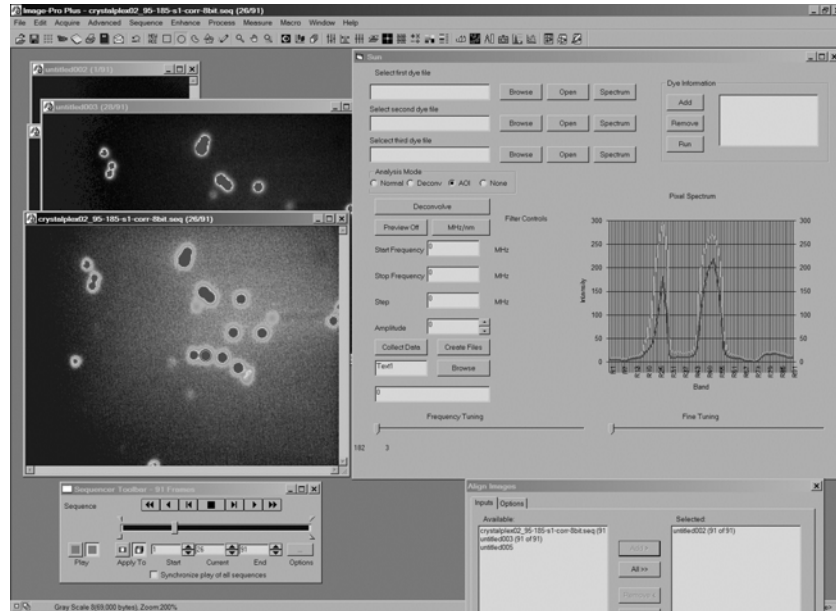


Figure 2 Multispectral image-acquisition module operating within the environment of Image Pro-Plus package.

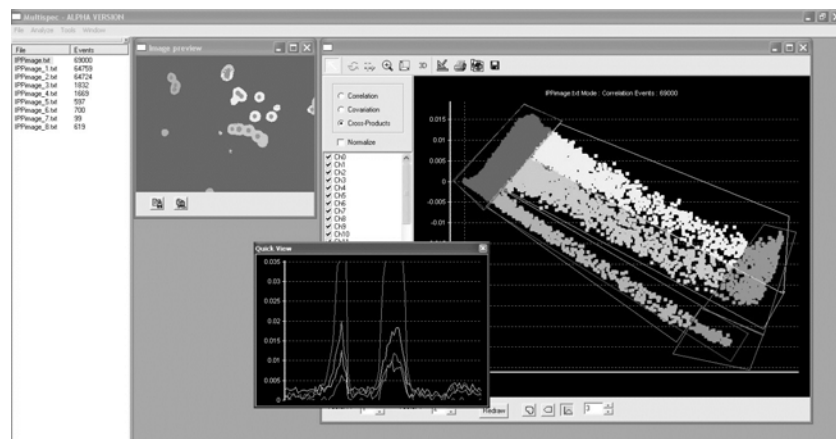


Figure 3 PCA-based analysis plug-in identifying different pixels on a multispectral image.

Figure 2 shows the acquisition part of our plug-in module, while Figure 3 demonstrates operation of the analytical component. In this example an image of latex beads labeled with quantum dots was processed using a PCA algorithm. Five different populations of pixels were automatically identified: the background pixels, the oversaturated pixels (in the centers of the beads), and pixels belonging to three different types of beads, representing different proportions of embedded red- and green-emitting nanocrystals.

3.3. Calibration

The system was calibrated using a multi-ion discharge lamp (MIDL; LightForm, Inc., Hillsborough, NJ) containing mercury ions and inorganic fluorophores as an absolute reference light source¹⁴. The MIDL emits stable, reproducible peaks between 400 and 650 nm. The lamp was positioned on the microscope stage below the objective lens. The characteristics of an acquired spectrum enabled us to measure wavelength accuracy, spectral sensitivity, and spectral resolution. The emission peaks were independently verified using a USB2000 spectrometer (Ocean Optics, Dunedin, FL). Figure 4 shows the spectra of the MIDL measured by USB2000 spectrometer and by our multispectral systems.

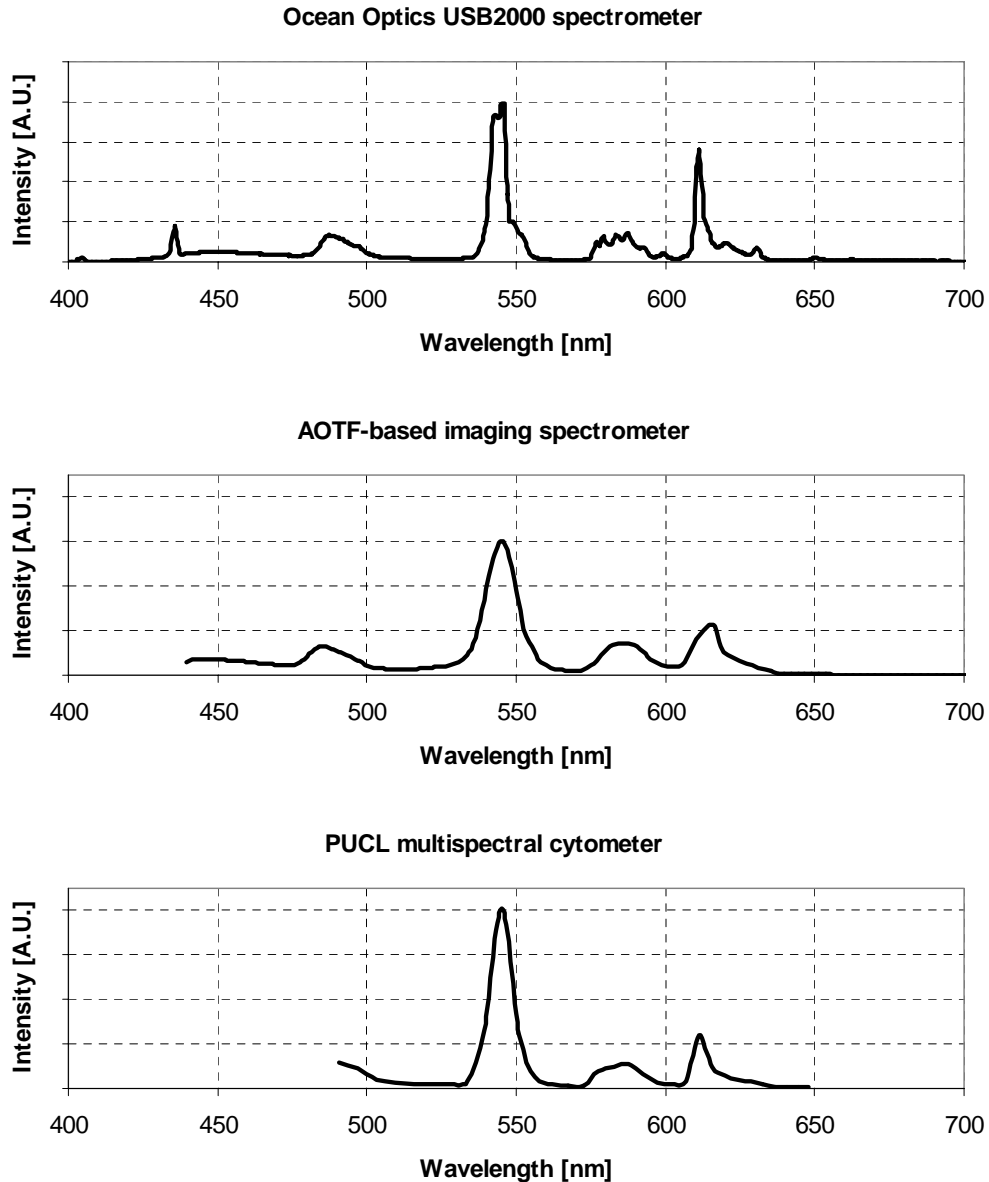


Figure 4 Readings of MIDL calibration spectrum obtained by Ocean Optics USB2000 spectrometer, AOTF-based imaging system equipped with QImaging Retiga 1300 camera, and PUCL multispectral cytometer equipped with Hamamatsu PMT7260 multianode PMT.

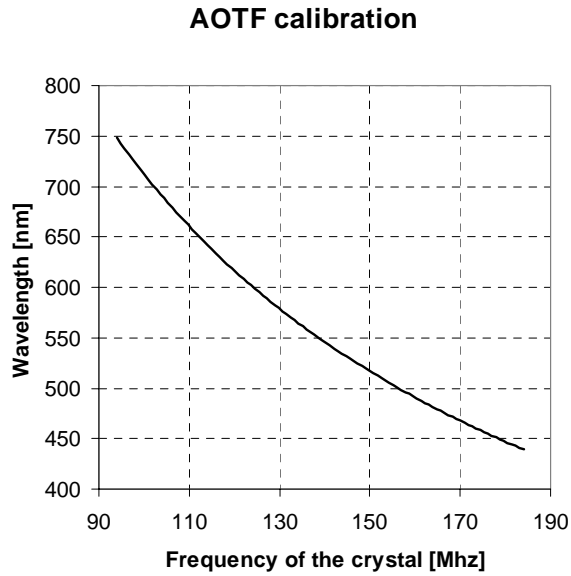


Figure 5 Spectral calibration plot of the TeO₂ AOTF filter based on multi-ion discharge lamp readings.

4. APPLICATIONS

The primary application of our system is verification of analyses provided by a newly developed multispectral flow cytometer (PUCL-MFC). This custom-built instrument capable of simultaneously collecting 32 bands of fluorescence between 400 and 880 nm (400 and 650 nm in the previous version) can be used for analysis of biological samples tagged with nanocrystal-based barcodes^{15,16} or organic fluorochromes with closely overlapping spectra². Since traditional fluorescence imaging is not capable of recognizing differences between fluorochromes with close spectra, it was not possible to verify PUCL-MFC observations independently. Figures below show an example in which lymphocytes were stained with two different stains with very similar spectra – DiBAC₄(3) (bis-(1,3-dibutylbarbituric acid)trimethine oxonol) and DiOC₆(3) (3,3'-dihexyloxycarbocyanine iodide). Whereas traditional fluorescence microscopy operating with a standard set of filters was not able to identify the differences recognized by PUCL-MFC, the multispectral system readily picked-up the distinction.

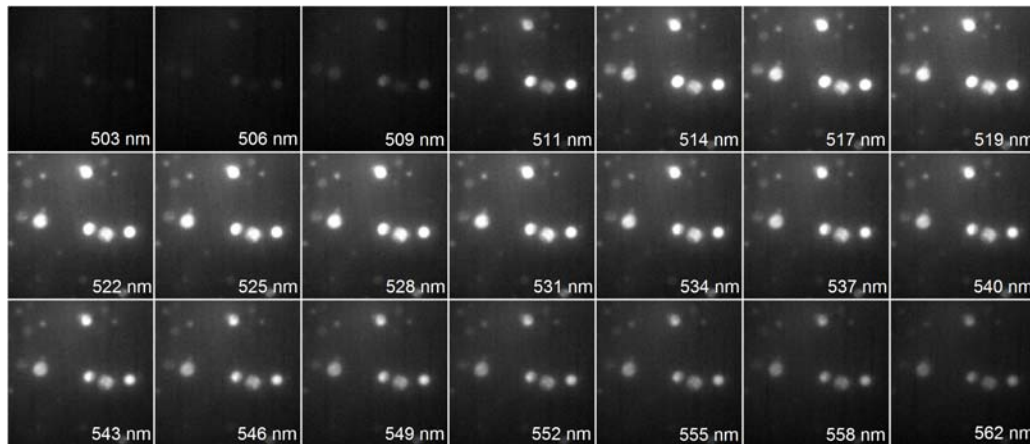


Figure 6 Set of monochrome images (spectral region 522 to 562 nm), showing lymphocytes stained with DiOC₆(3) and DiBAC₄(3). Images were collected using a Brimrose TeO₂ AOTF and a QImaging Retiga 1300 monochrome camera.

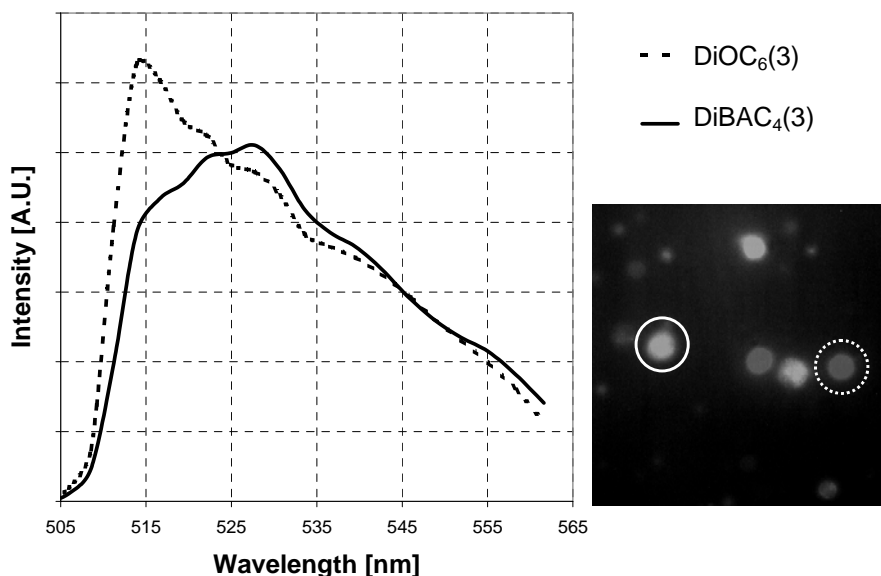


Figure 7 Spectra of lymphocytes recorded by the AOTF-based imaging system identify the presence of two different fluorochromes.

5. FURTHER DEVELOPMENT

Expanding the operating wavelength range of the AOTF is of great interest for many potential applications in the biological sciences. TeO_2 has a limited operating wavelength range, from 360 nm to 5000 nm, owing to its absorption. A UV AOTF can be made with other crystals, such as KDP (KH_2PO_4), while a mid-IR AOTF can use crystals like Hg_2Cl_2 to operate up to 20 μm .

The diffracted light intensity is directed into two physically separated first-order beams, denoted as the +1 and -1 beams. The angle between the beams is affected by the device design but is typically a few degrees. These beams are orthogonally polarized. When the incident beam is unpolarized, these two beams have nearly equal power. The efficiency of our current system is limited by the fact that only one polarization is utilized for imaging. Even though paratellurite efficiencies of 75-90% are possible, the actual efficiency becomes approximately half of the maximum possible. Increase in sensitivity can be achieved by projecting the two resulting images onto one CCD chip. It is also possible to extend the functionality of our system by projecting the +1 and -1 images onto two separate cameras, or two different areas of the same camera. In this case, simultaneous polarimetric and multispectral imaging would be possible.

6. CONCLUSIONS

In this report, we have presented an inexpensive and simple system for multi- and hyperspectral fluorescence/reflected light imaging. Although similar approaches were proposed for biological microscopy before¹⁷⁻²⁰ the maturation of acousto-optical technology, the availability of less expensive filters with larger apertures and the developments in CCD cameras now make the AOTF technology especially attractive. Since our control software operates within the environment of a popular image-acquisition and -processing package, the AOTF-based system can be very easily integrated with many existing fluorescence microscopes and cameras. We believe that the AOTF-based system may become an interesting alternative for more complex and expensive LCTF or pushbroom methods.

ACKNOWLEDGEMENTS

The authors wish to thank Crystalpex Corp. (Pittsburgh, PA) for providing the polystyrene microbeads tagged with red- and green-emitting nanocrystals.

REFERENCES

1. Martin, J.C., Yoshida, T.M. & Graves, S.W., "Spectral analysis flow cytometry," *Cytometry* **59A**, 30, 2004.
2. Robinson, J.P., Rajwa, B., Gregori, G.J., Jones, J.T. & Patsekine, V., "Collection hardware for high speed multispectral single particle analysis," *Cytometry* **59A**, 52, 2004.
3. Robinson, J.P., "Multispectral cytometry: the next generation," *Biophotonics International* **11**, 36-41, 2005.
4. Levenson, R.M. & Hoyt, C.C., "Spectral imaging and microscopy," *American Laboratory* **32**, 26-33, 2000.
5. Levenson, R., Cronin, P.J. & Pankratov, K.K. "Spectral imaging for brightfield microscopy" in *Spectral Imaging: Instrumentation, Applications, and Analysis II*. edited by Richard Levenson, Gregory H. Bearman & A. Mahadevan-Jansen, Proceedings of SPIE Vol. 4959 (SPIE, Bellingham, WA, 2003) pp. 27-33.
6. Levenson, R., "Spectral imaging for multicolor fluorescence and brightfield molecular studies," *Journal of Histochemistry & Cytochemistry* **52**, S15, 2004.
7. Lerner, J., Lu, T.T. & Vari, S.G. "Spectral topography of histopathological samples" in *Three Dimensional and Multidimensional Microscopy: Image Acquisition and Processing V*. edited by Carol J. Cogswell, Conchello Jose-Angel, Tony Wilson, Thomas T. Lu & Jeremy Lerner, Proceedings of SPIE Vol. 3261 (SPIE, Bellingham, WA, 1998) pp. 224-231.
8. Lerner, J. & Stein, L., "Hyperspectral imaging opens life-science vistas," *Laser Focus World* **34**, 89, 1998.
9. Dickinson, M.E., Bearman, G., Tille, S., Lansford, R. & Fraser, S.E., "Multi-spectral imaging and linear unmixing add a whole new dimension to laser scanning fluorescence microscopy," *Biotechniques* **31**, 1272-1276, 2001.
10. Bei, L., Dennis, G.I., Miller, H.M., Spaine, T.W. & Carnahan, J.W., "Acousto-optic tunable filters: fundamentals and applications as applied to chemical analysis techniques," *Progress in Quantum Electronics* **28**, 67-87, 2004.
11. Harris, S.E. & Wallace, R.W., "Acousto-optic tunable filter," *Journal of the Optical Society of America* **59**, 744-747, 1969.
12. Chang, I.C., "Analysis of the noncollinear acousto-optic filter," *Electronics Letters* **11**, 617-618, 1975.
13. Yano, T. & Watanabe, A., "Acoustooptic TeO₂ tunable filter using far-off-axis anisotropic Bragg diffraction," *Applied Optics* **15**, 2250-2258, 1976.
14. Lerner, J.M. & Zucker, R.M., "Calibration and validation of confocal spectral imaging systems," *Cytometry* **62A**, 8-34, 2004.
15. Han, M., Gao, X., Su, J.Z. & Nie, S., "Quantum-dot-tagged microbeads for multiplexed optical coding of biomolecules," *Nature Biotechnology* **19**, 631-635, 2001.
16. Chan, W.C., Maxwell, D.J., Gao, X., Bailey, R.E., Han, M. & Nie, S., "Luminescent quantum dots for multiplexed biological detection and imaging," *Current Opinions in Biotechnology* **13**, 40-46, 2002.
17. Flamion, B., Bungay, P.M., Gibson, C.C. & Spring, K.R., "Flow rate measurements in isolated perfused kidney tubules by fluorescence photobleaching recovery," *Biophysics Journal* **60**, 1229-1242, 1991.
18. Wachman, E.S., Wen-Hua, N. & Farkas, D.L., "Imaging acousto-optic tunable filter with 0.35-micrometer spatial resolution," *Applied Optics* **35**, 5220-5226, 1996.
19. Wachman, E.S., Niu, W. & Farkas, D.L., "AOTF microscope for imaging with increased speed and spectral versatility," *Biophysics Journal* **73**, 1215-1222, 1997.
20. Morris, H.R., Hoyt, C.C. & Treado, P.J., "Imaging Spectrometers for Fluorescence and Raman Microscopy - Acoustooptic and Liquid-Crystal Tunable Filters," *Applied Spectroscopy* **48**, 857-866, 1994.